A* layers with respect to each other. The resultant phase is referred to as a twist grain boundary (TGB) phase. They predicted this phase can occur between the cholesteric and the smectic A phase in a way similar to how the Abrikosov flux lattice phase can occur between the normal and the superconducting phases.[28] Renn and Lubensky further established that the requirement for this intermediate phase to occur is that the Ginzburg parameter, which is equal to the ratio of the twist penetration length (λ_T) to the smectic A correlation length (ξ), must ge greater than $1/2^{1/2}$.

Thus, the TGB phase could be a feasible model for the smectic A* phase, for the following reasons. First, the X-ray scattering predicted for the TGB phase is consistent with our X-ray measurements on the A* phase. Second, the model predicts a helical structure with a helical axis parallel to the smectic layers, which is consistent with our optical experiments. Last, we observe the A* phase in the vicinity of a smectic A to smectic C* transition where the A phase has a short temperature range. At such a transition, λ_T diverges, which results in a large value for the Ginzburg parameter, as required by the theory.[29] Hence, the TGB phase is a viable model for the A* phase. As a consequence, we can explore the implications of this possibility still further, and in particular, we can speculate on the nature of the effect observed between the A* phase and the isotropic phase. For the superconducting flux lattice it has been proposed,[30] and observed,[31] that the vortex lattice can disorder into an entangled or disentangled fluid of vortexes. We suggest that a similar disordering of the regular array of screw dislocations in the TGB phase may be the mechanism responsible for the occurrence of the phase observed in the isotropic liquid just above the A* phase.

Finally, we should make some comments on the use of the notation A* to describe the new phase. Without the presence of optically active material the smectic A phase is a nonchiral phase. However, if the phase contains chiral molecules the phase can become chiral. This can be achieved by perturbing the structure of the phase in an applied field or by distorting the structure mechanically. In both of these situations the symmetry of the phase is broken, resulting in electroclinic or flexoelectric behavior. In the new phase the symmetry is also broken by the helical structure, but in this case it is not achieved by external forces. Therefore, the phase can be appropriately designated A*. However, the complications involving space symmetry and helicity in these mesophases show that the nomenclature system is in need of serious review.

(28) Abrikosov, A. A. *Sov. Phys.—JETP (Engl. Transl.)* **1957**, *5*, 1174.
(29) Meyer, R. B., personal communication.
(30) Nelson, D. R. *Phys. Rev. Lett.* **1988**, *60*, 1973.
(31) Gammel, P. L.; Bishop, D. J.; Dolan, G. J.; Kwo, J. R.; Murray, C. A.; Schneemeyer, L. F.; Waszaczak, J. *Phys. Rev. Lett.* **1987**, *59*, 2592.

Summary

We have discovered a new helical liquid crystal and have shown that it is analogous to a twisted smectic A phase. Therefore we have classified the phase as smectic A*. The helix was found to propagate in a direction parallel to the layers, thereby producing twist distortions within the layers. It is suggested that these distortions are possibly organized into a lattice of screw dislocations.

Acknowledgment. We thank Professors T. Lubensky and R. Meyer for stimulating discussions.

Registry No. (*R*)-$C_8H_{17}O$-*p*-C_6H_4-C≡CCOO-*p*-C_6H_4-*p*-C_6H_4-$COOCH(CH_3)C_6H_{13}$, 122521-57-7; (*S*)-$C_8H_{17}O$-*p*-C_6H_4-C≡CCOO-*p*-C_6H_4-*p*-C_6H_4-$COOCH(CH_3)C_6H_{13}$, 122521-61-3; (*R*)-$C_9H_{19}O$-*p*-C_6H_4-C≡CCOO-*p*-C_6H_4-*p*-C_6H_4-$COOCH(CH_3)C_6H_{13}$, 122521-58-8; (*S*)-$C_9H_{19}O$-*p*-C_6H_4-C≡CCOO-*p*-C_6H_4-*p*-C_6H_4-*p*-C_6H_4-$COOCH(CH_3)C_6H_{13}$, 122521-62-4; (*R*)-$C_{10}H_{21}O$-*p*-C_6H_4-C≡CCOO-*p*-C_6H_4-*p*-C_6H_4-$COOCH(CH_3)C_6H_{13}$, 122521-59-9; (*S*)-$C_{10}H_{21}O$-*p*-C_6H_4-C≡CCOO-*p*-C_6H_4-*p*-C_6H_4-$COOCH(CH_3)C_6H_{13}$, 122521-63-5; (*R*)-$C_{11}H_{23}O$-*p*-C_6H_4-C≡CCOO-*p*-C_6H_4-*p*-C_6H_4-$COOCH(CH_3)C_6H_{13}$, 122521-60-2; (*S*)-$C_{11}H_{23}O$-*p*-C_6H_4-C≡CCOO-*p*-C_6H_4-*p*-C_6H_4-$COOCH(CH_3)C_6H_{13}$, 122521-64-6; (*R*)-$C_{12}H_{25}O$-*p*-C_6H_4-C≡CCOO-*p*-C_6H_4-*p*-C_6H_4-$COOCH(CH_3)C_6H_{13}$, 120551-07-7; (*S*)-$C_{12}H_{25}O$-*p*-C_6H_4-C≡CCOO-*p*-C_6H_4-*p*-C_6H_4-$COOCH(CH_3)C_6H_{13}$, 122521-65-7; (*R*)-$C_{13}H_{27}O$-*p*-C_6H_4-C≡CCOO-*p*-C_6H_4-*p*-C_6H_4-$COOCH(CH_3)C_6H_{13}$, 120551-01-1; (*S*)-$C_{13}H_{27}O$-*p*-C_6H_4-C≡CCOO-*p*-C_6H_4-*p*-C_6H_4-$COOCH(CH_3)C_6H_{13}$, 120551-04-4; (*R*)-$C_{14}H_{29}O$-*p*-C_6H_4-C≡CCOO-*p*-C_6H_4-*p*-C_6H_4-$COOCH(CH_3)C_6H_{13}$, 120551-02-2; (*S*)-$C_{14}H_{29}O$-*p*-C_6H_4-C≡CCOO-*p*-C_6H_4-*p*-C_6H_4-$COOCH(CH_3)C_6H_{13}$, 120551-05-5; (*R*)-$C_{15}H_{31}O$-*p*-C_6H_4-C≡CCOO-*p*-C_6H_4-*p*-C_6H_4-$COOCH(CH_3)C_6H_{13}$, 120551-03-3; (*S*)-$C_{15}H_{31}O$-*p*-C_6H_4-C≡CCOO-*p*-C_6H_4-*p*-C_6H_4-$COOCH(CH_3)C_6H_{13}$, 120551-06-6; (*R*)-$C_{16}H_{33}O$-*p*-C_6H_4-C≡CCOO-*p*-C_6H_4-*p*-C_6H_4-$COOCH(CH_3)C_6H_{13}$, 120551-08-8; (*S*)-$C_{16}H_{33}O$-*p*-C_6H_4-C≡CCOO-*p*-C_6H_4-*p*-C_6H_4-$COOCH(CH_3)C_6H_{13}$, 122521-66-8.

Palladium Carbonyl Clusters Entrapped in NaY Zeolite Cages: Ligand Dissociation and Cluster–Wall Interactions

Lien-Lung Sheu, Helmut Knözinger,† and Wolfgang M. H. Sachtler*,‡

Contribution from the V.N. Ipatieff Laboratory, Center for Catalysis and Surface Science, Northwestern University, Evanston, Illinois 60208. *Received April 13, 1989*

Abstract: Highly structured FTIR spectra, which are indicative of Pd carbonyl clusters, are obtained after adsorption of CO on Pd/NaY which was reduced at 200 °C, but broad IR bands are observed with samples which were reduced at higher temperatures. Pd carbonyl clusters with only CO ligands have not been reported previously, which indicates that the geometry of NaY supercages favors their formation. As the clusters lose some of their CO ligands, old IR bands erode and new IR bands with sharp isosbestic points emerge. This process is entirely reversed upon reintroduction of CO. The low activation energy of CO release and concomitant changes in the IR band characteristic of zeolite O–H vibrations indicate a chemical interaction of zeolite protons and Pd carbonyl clusters.

Zeolite-supported, highly dispersed metal catalysts have steadily gained importance since the pioneering work by Rabo et al.[1] The combination of the catalytic properties of transition metals with the steric constraints imposed by the zeolite structure carries great potential for active and selective catalysts. A combination of

† Institut für physikalische Chemie der Universität München, West Germany
‡ Present address: Technical Center, The BOC Group, Inc., 100 Mountain Avenue, Murray Hill, New Jersey 07974.

(1) Rabo, J. A.; Pickert, P. E.; Mays, R. L. *Ind. Eng. Chem.* **1961**, *53*, 733.

0002-7863/89/1511-8125$01.50/0

physical techniques (XRD, EXAFS) and chemical methods (e.g., temperature-programmed reduction, H_2 chemisorption, and its temperature-programmed desorption) has been used[2,3] to characterize and control the location and the average size of zeolite-entrapped metal particles. Recently, it was discovered[4] that very detailed information on the Pd particles in NaY can be obtained from FTIR of adsorbed CO: highly structured spectra are obtained for samples reduced at 200 °C, but spectra with broad bands, reminiscent of CO adsorbed on conventional supported Pd catalysts,[5] are observed for samples reduced, e.g., at 500 °C. The former FTIR spectra, exhibiting very sharp bands, have been attributed to a palladium carbonyl cluster, possibly with a core of 13 Pd atoms.[4] This cluster would perfectly fit in the supercages of NaY. Thus far, no Pd clusters having exclusively CO ligands have been reported in the literature, but mixed carbonyl–phosphine Pd clusters were reported by Mednikov et al.[6] Apparently, the environment of a faujasite supercage is favorable for formation and/or stabilization of carbonyl clusters. The so-called "ship-in-a-bottle" technique has been applied to synthesize various organometallic clusters which have ever been synthesized outside the zeolite cages. Herron et al.[7] prepared mixed Ni carbonyl phosphines in zeolite X by $Ni(CO)_4$ and trimethyl- or triethylphosphine. Bein et al.[8] prepared mixed Ni complexes containing Ni^0 and Ni^{2+} with CO and phosphine ligands.

Other zeolite encaged metal carbonyl complexes, which have been synthesized outside the zeolite cages, include Rh and Ir carbonyls. Pioneering work was done by Gelin et al.[9] and Bergeret et al.[10] with Rh complexes in zeolites. Mantovani et al.[11] report transformation of $Rh_4(CO)_{12}$ into $Rh_6(CO)_{16}$. For Ir complexes, Bergeret et al.[12] found that $Ir_6(CO)_{16}$ formed after reacting a CO/H_2O or CO/H_2 mixture at 440–470 K on $Ir^{III}Y$ zeolite. Gelin et al. state that $Ir_4(CO)_{12}$ is formed under milder conditions in NaY than in solution, again suggesting that zeolite cages favor thermodynamically and/or kinetically the formation of some metal carbonyl complex.

The kinetic behavior of the zeolite encapsulated Pd carbonyl cluster is intriguing and can be clearly monitored by FTIR; CO is released at low temperature and new bands emerge, which are separated from the vanishing bands by sharp isosbestic points.[4] In the present paper we report a first analysis of the interaction of entrapped complexes with gaseous CO and with the zeolite

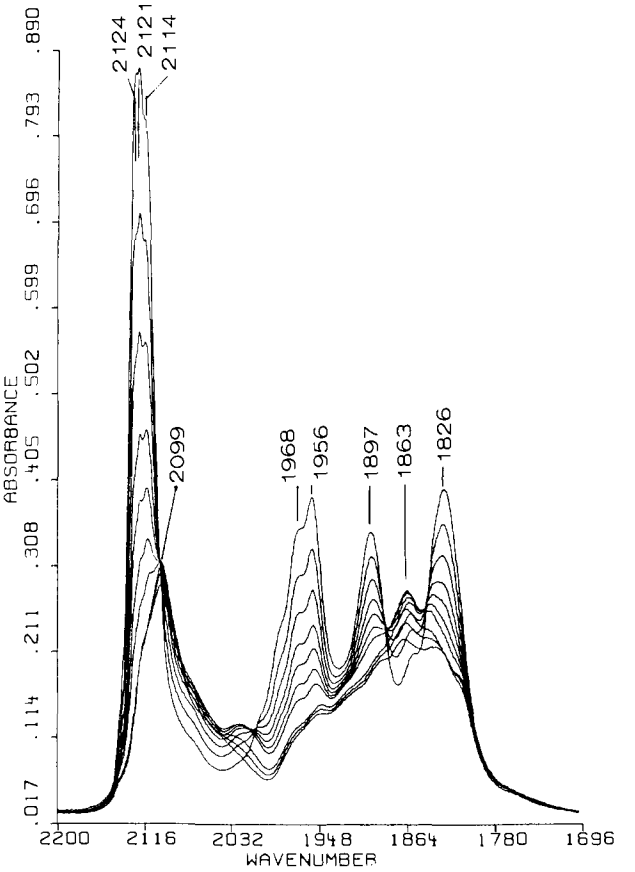

Figure 1. FTIR spectra of CO adsorbed on $Pd_4NaY(500/100/60)$ after different purging times with Ar at 25 °C. Purging time (min): 20, 25, 30, 35, 40, 45, 50, 70, 80, 100.

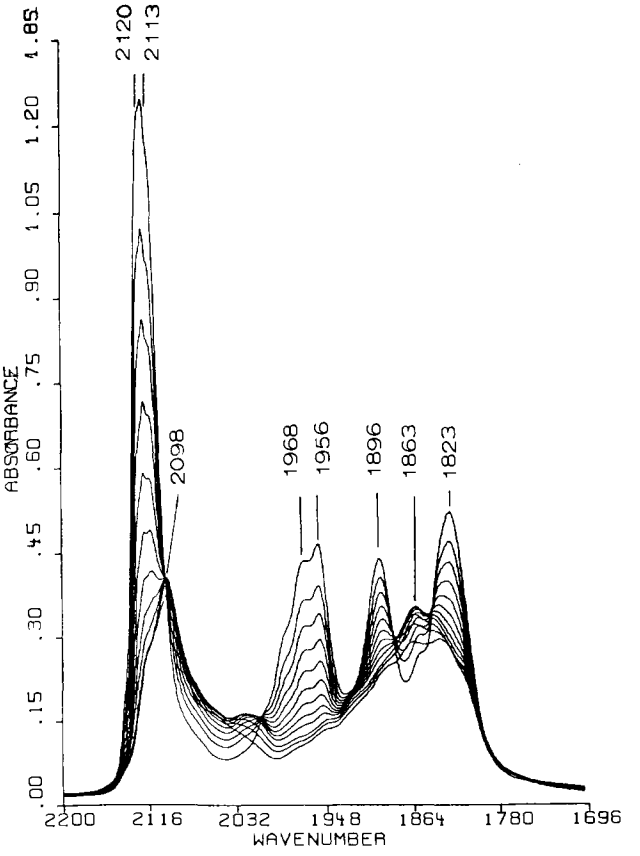

Figure 2. FTIR spectra of CO adsorbed on $Pd_4NaY(500/200/20)$ after different purging times with Ar at 25 °C. Purging time (min): 20, 25, 30, 35, 40, 45, 50, 55, 60, 70, 80, 100.

(2) (a) Tzou, M. S.; Teo, B. K.; Sachtler, W. M. H. *J. Catal.* **1988**, *113*, 220. (b) Moretti, G.; Sachtler, W. M. H. *J. Catal.* **1989**, *115*, 205. (c) Moretti, G.; Sachtler, W. M. H. *J. Catal.* **1989**, *115*, 205. (d) Balse, V. R.; Sachtler, W. M. H.; Dumesic, J. A. *Catal. Lett.* **1988**, *1*, 275. (e) Tzou, M. S.; Jiang, H. J.; Sachtler, W. M. H. *React. Kinet. Catal. Lett.* **1987**, *35*, 207. (f) Park, S. H.; Tzou, M. S.; Sachtler, W. M. H. *Appl. Catal.* **1986**, *24*, 85. (g) Tzou, M. S.; Jiang, H. J.; and Sachtler, W. M. H. *Appl. Catal.* **1986**, *20*, 231. (h) Tzou, M. S.; Jiang, H. J.; Sachtler, W. M. H. *Langmuir* **1986**, *2*, 773. (i) Jiang, H. J.; Tzou, M. S.; Sachtler, W. M. H. *Appl. Catal.* **1988**, *39*, 255.

(3) (a) Homeyer, S. T.; Sachtler, W. M. H. *J. Catal.* **1989**, *116*, 91. (b) Homeyer, S. T.; Sachtler, W. M. H. *J. Catal.* **1989**, *118*, 266. (c) Homeyer, S. T.; Sachtler, W. M. H. *Appl. Catal.*, in press. (d) Homeyer, S. T.; Sachtler, W. M. H. In *Zeolites, Facts, Figures, Future*; Jacobs, P. A., Van Santen, R. A., Eds.; Elsevier: Amsterdam, p 975.

(4) Sheu, L. L.; Knözinger, H.; Sachtler, W. M. H. *Catal. Lett.* **1989**, *2*, 129.

(5) (a) For an excellent review article see: Sheppard, N.; Nguyen, T. T. In *Advances in Infrared and Raman Spectroscopy*; Clark, R. J. H., Hester, R. E., Eds.; Heyden: London, 1978; Vol. 5. (b) Sheu, L. L.; Karpinski, Z.; Sachtler, W. M. H. *J. Phys. Chem.* **1989**, *93*, 4890.

(6) Mednikov, E.; Eremenko, N. K.; Gubin, S. P.; Slovokhotov, Yu. L.; Struchkov, Yu. T. *J. Organomet. Chem.* **1982**, *239*, 401.

(7) Herron, N.; Stuckey, G. D.; Tolman, C. A. *Inorg. Chim. Acta* **1985**, *100*, 135.

(8) Bein, Th.; McLain, S. J.; Corbin, D. R.; Farley, R. D.; Moller, K.; Stuckey, G. D.; Woolery, G.; Sayers, D. *J. Am. Chem. Soc.* **1988**, *110*, 1801.

(9) Gelin, P.; Lefebvre, F.; Elleuch, B.; Naccache, C.; Ben Taarit, Y. In *Intrazeolite Chemistry* (ACS Symposium Series No. 218); Stucky, D., Dwyer, F. G., Eds.; American Chemical Society: Washington, DC, 1983; p 455.

(10) Bergeret, G.; Gallezot, P.; Gelin, P.; Ben Tarrit, Y.; Lefebvre, L., Naccache, C.; Shannon, R. D. *J. Catal.* **1987**, *104*, 279.

(11) Mantovani, E.; Palladino, N.; Zanobi, A. *J. Mol. Catal.* **1977/80**, *3*, 285.

(12) Bergeret, G.; Gallezot, P.; Lefebvre, F. *Proc. Int. Conf. Zeolites, 7th* **1986**, 401.

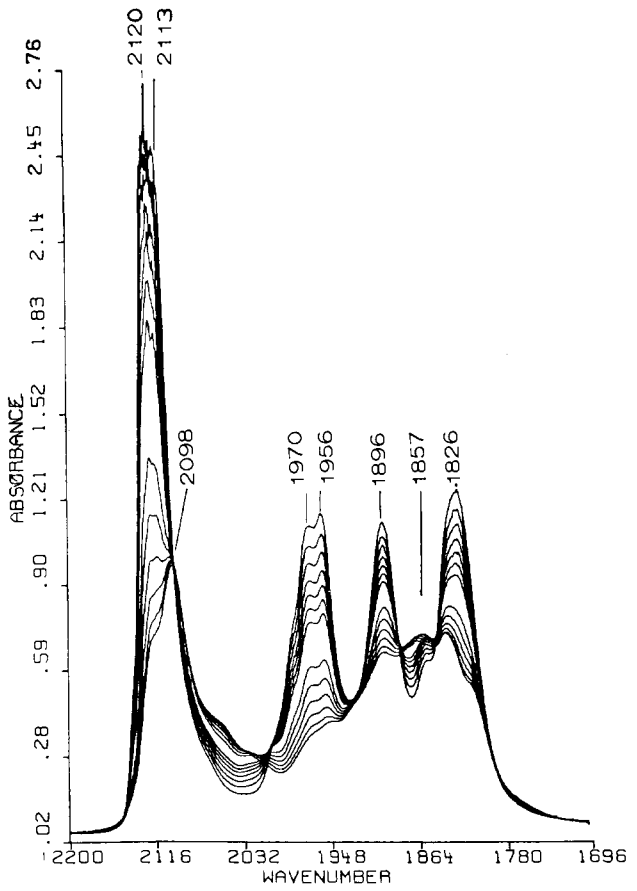

Figure 3. FTIR spectra of CO adsorbed on $Pd_4NaY(500/350/20)$ after different purging times with Ar at 25 °C. Purging time (min): 20, 25, 30, 35, 40, 50, 60, 90, 100, 110, 120, 130, 150.

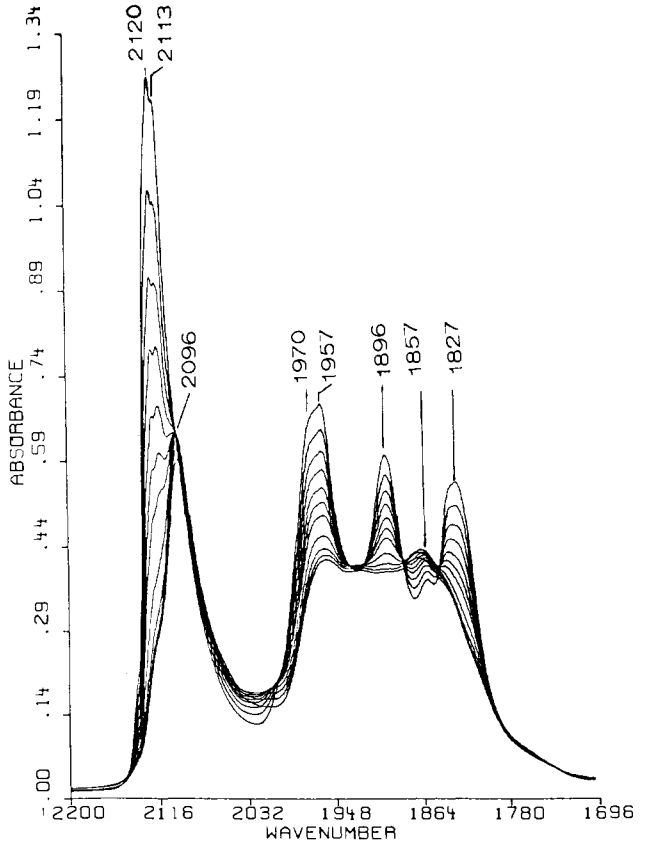

Figure 4. FTIR spectra of CO adsorbed on $Pd_4NaY(500/350/300)$ after different purging times with Ar at 25 °C. Purging time (min): 20, 25, 30, 35, 40, 45, 50, 60, 70, 80, 90.

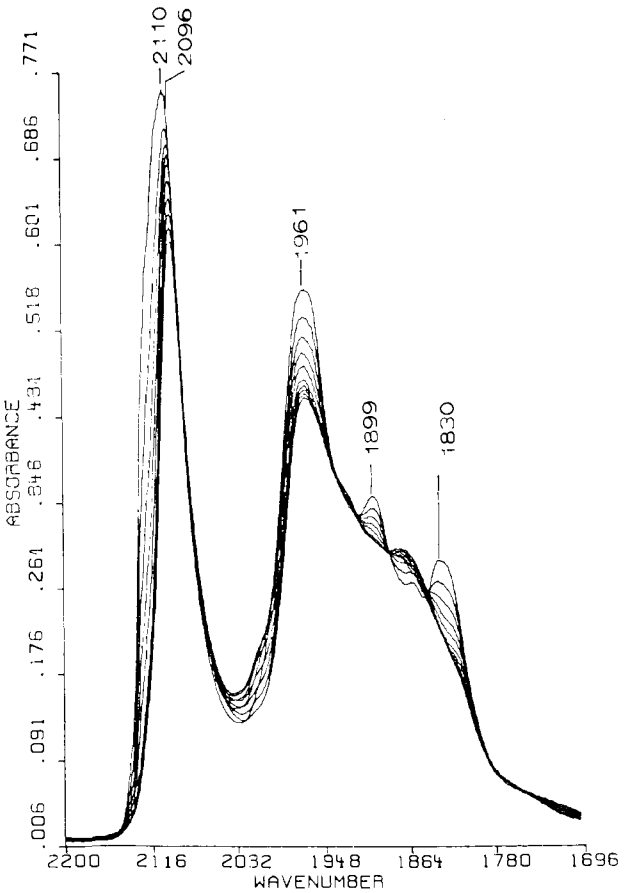

Figure 5. FTIR spectra of CO adsorbed on $Pd_4NaY(500/500/60)$ after different purging times with Ar at 25 °C. Purging time (min): 20, 25, 30, 35, 40, 50, 60, 70, 80, 90.

protons, which are formed during reduction of ion-exchanged Pd ions with H_2.

Experimental Section

Pd/NaY samples were prepared by ion exchange of Linde NaY (LZY-52, Lot No. 968083061080-S-9, $Na_{57}(AlO_2)_{57}(SiO_2)_{135}\cdot 375H_2O$), in a dilute aqueous solution of $[Pd(NH_3)_4](NO_3)_2$ (Strem Chemicals, Lot No. 19167). The catalyst was then calcined in flowing oxygen of 1 atm at a temperature increasing from 20 °C to the specified calcination temperature (T_C) at a rate of 0.5 °C/min, then held at T_C for 2 h. The calcined sample (20 mg) was pressed into 10-mm diameter wafers, then transferred to the IR quartz cell and reduced in situ with 1 atm of H_2 flow.

After the H_2 was replaced by flowing Ar for 20 min at the reduction temperature, the samples were cooled to room temperature in Ar. An FTIR spectrum, serving further as the background spectrum, was recorded by a Nicolet 60SX single-beam Fourier transform IR spectrometer (resolution 1 cm^{-1}). The samples were then exposed to a flow of pure CO (1 atm) for 10 min, and the IR spectra were recorded. After subsequent purging with Ar, more IR spectra were taken while the CO coverage decreased. Generally, 200 scans were used for each spectrum to obtain satisfactory signal/noise ratios with each spectrum taking about 2.5 min; the recording was continuously ratioed with the background spectrum. The Pd loading and treatment conditions of each sample are denoted by $Pd_nNaY(T_C/T_R/t_r)$, in which the experimental variables are n (number of Pd atoms/unit cell of NaY), T_C (calcination temperature in °C), T_R (reduction temperature in °C), and t_r (reduction time in min). Experimental conditions are described in detail in ref 4.

Results

The CO–FTIR spectra of the samples $Pd_4NaY(500/100/60)$, $Pd_4NaY(500/200/20)$, $Pd_4NaY(500/350/20)$, $Pd_4NaY(500/350/300)$, $Pd_4NaY(500/500/60)$, and $Pd_4NaY(500/500/300)$, respectively, are shown in Figures 1–6. The effect of the reduction temperature on the CO–FTIR spectra is dramatic. After mild reduction the CO–FTIR spectra show sharp bands, but samples which were reduced at high temperature show broad bands, similar to the familiar CO–IR spectra of Pd/SiO_2. The spectra for the

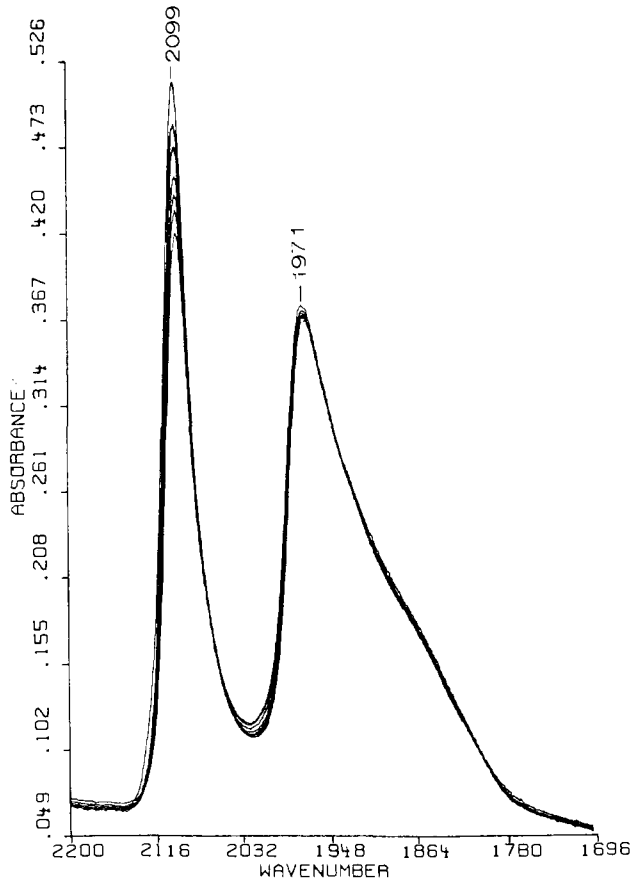

Figure 6. FTIR spectra of CO adsorbed on $Pd_4NaY(500/500/300)$ after different purging times with Ar at 25 °C. Purging time (min): 20, 25, 30, 40, 50, 60, 80.

Table I. Carbonyl Stretching Band Positions (cm^{-1}) for Entrapped Pd Clusters after Various Treatments

sample	state I	state II
$Pd_4NaY(500/100/60)$	2124, 2121, 2114 1968, 1956 1897, 1826	2099, 1863
$Pd_4NaY(500/200/20)$	2120, 2113 1968, 1956 1896, 1823	2098, 1863
$Pd_4NaY(500/350/20)$	2120, 2113 1970, 1956 1896, 1826	2098, 1857
$Pd_4NaY(500/350/20)$	2120, 2113 1970, 1956 1896, 1826	2098, 1857
$Pd_4NaY(500/350/300)$	2120, 2113 1970, 1957 1896, 1827	2096, 1857
$Pd_4NaY(500/500/60)$	2110 1961, 1899, 1830	2096
$Pd_4NaY(500/500/300)$	2099, 1971	

$Pd_4NaY(500/350/20)$ sample with different degrees of CO release are displayed in Figure 7a with shifted baselines for better distinction; the difference spectra of the same sample are shown in Figure 7b. They demonstrate the erosion of the original bands at 2114, 1969, 1956, 1900, and 1824 cm^{-1}, which are characteristic for high CO coverage, but also the simultaneous emergence and growth of a new band at 1860 cm^{-1} and of the features between 2060 and 2100 cm^{-1}. As more CO is removed, these features also wane. We shall further denote the state of high CO coverage as state I and the final stage after extended purging as state II. Their C–O stretching frequencies for different samples are summarized in Table I. Once state II is reached, further Ar purging causes all peaks to decrease steadily.

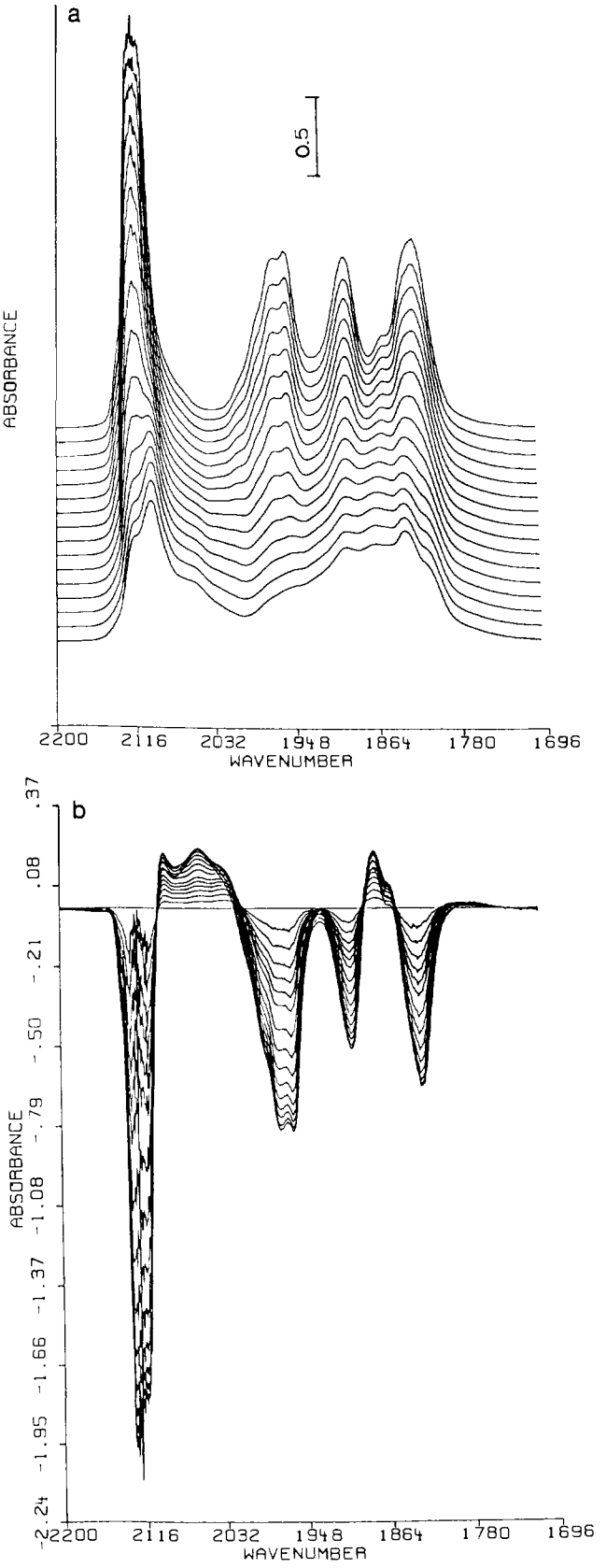

Figure 7. (a) Spectra of CO on $Pd_4NaY(500/350/20)$ after different purging times (listed in the caption of figure 3) with Ar, shown with shifted base lines. (b) Difference spectra of CO adsorbed on $Pd_4NaY(500/350/20)$, based on the spectrum of 20 min of Ar purging.

An experiment was carried out to test the extent of reversibility of the observed phenomena. After a first CO admission and desorption cycle, the sample $Pd_4NaY(500/350/20)$ was reexposed to 1 atm of CO; then the CO release was again monitored by

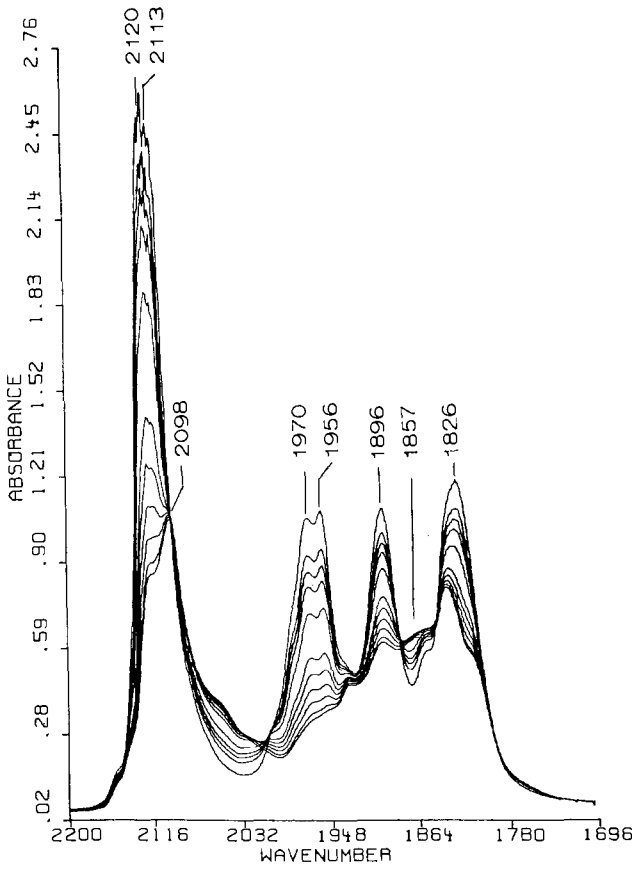

Figure 8. FTIR spectra of CO adsorbed on $Pd_4NaY(500/350/20)$ in second CO adsorption/desorption cycle. Ar purging time (min): 20, 30, 35, 40, 50, 70, 80, 90, 100, 110, 120.

FTIR. The spectra for the second cycle, shown in Figure 8, are quantitatively identical with those of Figure 3. We conclude that no irreversible structure modifications were induced by CO in the first adsorption/desorption cycle. Reintroduction of CO in the second cycle causes not only those bands (2114, 1969, 1956, 1900, 1824 cm^{-1}) which had been eroded during CO release in the first cycle to grow again to their original intensity in state I, but, most remarkably, the new bands which had emerged when CO was released now disappear when CO is readsorbed. We will discuss this astounding finding in detail in the Discussion section.

Accompanying the changes in CO coverage of the Pd particles were changes in the bands due to the zeolite O–H stretching vibrations. FTIR spectra in the 3800–3200-cm^{-1} region are presented in Figure 9 for $Pd_4NaY(500/350/20)$. A strong peak at 3645 cm^{-1} and a weak broad peak around 3500 cm^{-1} are observed when the sample is in state I (high CO coverage of Pd); they are attributed to the vibrational peaks of hydroxyl groups, consistent with the protons, which are formed by the reduction of Pd^{2+} ions with H_2, becoming attached to O^- ions of zeolite cage walls. As the sample was purged with Ar, the intensity of these bands decreased in synchronism with the decreasing CO bands, suggesting that protons are consumed when CO is released from Pd clusters. It is remarkable that this phenomenon is also reversible; upon introducing CO in the second cycle, the zeolite hydroxyl group bands recovered their original intensity, and this intensity decayed again during the second Ar purging. The corresponding absorbance values are 0.66 for state I (spectrum 9a), 0.365 for state II (spectrum 9c), and, again, 0.660 for state I (spectrum 9d). Also the shift of the position of the stronger band is clearly detectable, despite the inevitable noise level in this spectral region, namely, from 3647 cm^{-1} (Figure 9a) to 3639 cm^{-1} (Figure 9c) and back to 3647 cm^{-1} (Figure 9d).

Blank experiments confirmed the absence of significant CO adsorption on the metal-free zeolite NaY; the highest intensity detected after purging gaseous CO for 20 min was less than 0.001.

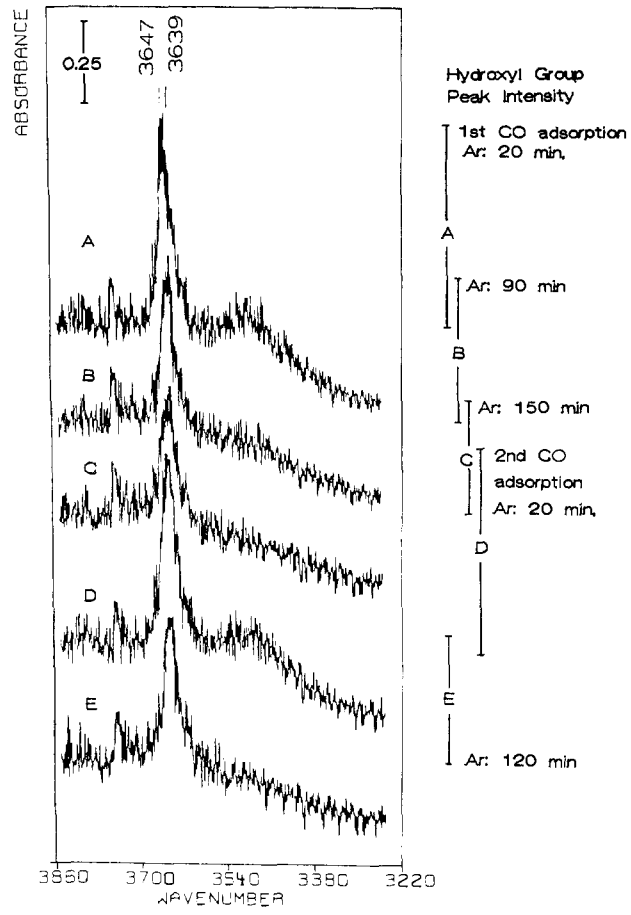

Figure 9. FTIR spectra of hydroxyl group in $Pd_4NaY(500/350/20)$ after various purging times (min) with Ar at 25 °C: (a) 20, (b) 90, (c) 150, (d) 20, (e) 120; (a–c) after first adsorption; (d,e) after purging for 150 min and readmission of CO.

Discussion

The results are interpreted on the basis of the following assumptions. The CO–IR spectra of the samples that were reduced at low temperature (shown in Figures 1 and 2) are predominantly due to Pd clusters with carbonyl ligands located inside supercages of NaY. The $Pd_{13}(CO)_x$ carbonyl serves as a prototype for these. The spectrum in Figure 6 of the sample which was reduced at 500 °C is typical for CO adsorption on fairly large Pd particles; these are presumably located at the external surface of NaY or in voids, where the zeolite lattice has collapsed.[13] These assumptions are based on the positions and shapes of the IR bands in comparison to spectra of other well-defined Pd samples. Of particular relevance are the IR spectra of CO on Pd single-crystal faces, reported by Bradshaw and Hoffman;[14] their data justify our conclusion that the narrow band at 2120 cm^{-1} in Figure 1 corresponds to terminal CO, whereas the band at 1896 cm^{-1} is attributed to doubly bridging CO, and the band at 1823 cm^{-1} to triply bridging CO. Further, the synchronized disappearance of the 1969- and 1950-cm^{-1} bands during purging suggests that they belong to one species, possibly a pair of bridging CO ligands in a "butterfly" arrangement involving two adjacent Pd atoms. These band assignments were made previously.[4] The geometry of the NaY supercages suggests that the core of the clusters could consist of 13 Pd atoms; such clusters including the bridging CO ligands would perfectly fit inside these cages, while the terminal CO ligands would point outward through cage windows. Indeed, an analogous Rh_{13} hydrido carbonyl cluster with 13 Rh atoms in cubooctahedral (hcp) arrangement is reported in the literature.[15]

(13) Bergeret, G.; Gallezot, P.; Imelik, B. *J. Phys. Chem.* **1981**, *85*, 411.
(14) (a) Bradshaw, A. M.; Hoffmann, F. *Surf. Sci.* **1978**, *72*, 513. (b) Bradshaw, A. M.; Hoffmann, F. *Surf. Sci.* **1975**, *52*, 449.

The TEM pictures of Pd/Al_2O_3 reported by Schmid et al.[16] offer another direct evidence of preferred formation of 13-atom Pd clusters on Pd/Al_2O_3. Bergeret et al. detected 5–7-Å particles in $Pd_{13.7}Na_{9.3}H_{19.2}/Y$ by SAXS after calcination at 600 °C and H_2 reduction at 150 °C.[17] EXAFS data[18] of $Pd_4NaY(500/350/20)$ show a coordination number of about 6. These results offer the indirect evidence to support our 13-atom Pd cluster model. To our knowledge, no Pd clusters exclusively covered with carbonyl ligands have ever been reported; the present observation suggests that the cage geometry significantly favors the formation of such clusters.

In the present paper attention is focused on three issues: (1) the effect of the reduction temperature on the formation of the Pd clusters, prior to admission of CO; (2) the formation of electron-deficient Pd; and (3) the chemistry responsible for CO release by Ar purging at room temperature.

From previous results[3,13] it is known that calcination at 500 °C of ion-exchanged Pd/NaY places the Pd^{2+} ions quantitatively in the sodalite cages; their reduction is incomplete at 100 °C, but complete at 320 °C. Pd atoms or dimers are formed which are first trapped in these cages but escape to supercages at a rate that depends on T_R. Once Pd atoms arrive in supercages, they can easily agglomerate to small clusters; these grow further by trapping atoms escaping from sodalite cages or by collision with other clusters. Migration is fast until the critical cluster size is reached after which its passage through the 7-Å window becomes impossible. CO probes for Pd clusters in supercages, but Pd atoms in $S_{II'}$ sites may also form bonds with CO through the six-membered oxygen ring between supercage and sodalite cage. In conformity with this model, the present data (see Figures 1, 2, and 3) show that the absorbance of all IR bands increases with T_R up to T_R = 350 °C, reflecting both the increase of the fraction of Pd which is reduced and of the fraction of the reduced Pd which is located in supercages as clusters. This perfectly matches earlier dispersion measurements of Homeyer et al.[3] for the same samples: H/Pd_s = 0.63 for $Pd_4NaY(500/200/20)$, but H/Pd_s = 0.78 for $Pd_4NaY(500/350/20)$.

Before reduction is complete, some Pd might be present as Pd^+ in small cages. Electron-deficient Pd can also arise from interaction of Pd atoms or Pd_n clusters with protons; XRD results of Bergeret et al.[13,17] suggest that a significant proportion of reduced Pd atoms is retained within sodalite cages occupying $S_{II'}$ sites where Pd can be polarized by protons. The presence of $Pd^{\delta+}$ and Pd^+ ions is indeed suggested by the present CO–IR spectra, in particular, in the terminal C–O stretching region around 2124 cm^{-1}. This spectral region is shown in Figure 10 with expanded wavenumber scale for $Pd_4NaY(500/100/60)$. Three overlapping bands are clearly seen at 2125, 2121, and 2114 cm^{-1} in state I, as well as a band at 2100 cm^{-1} in state II; these bands show significantly different behavior during CO desorption. From a comparison of the band positions with literature data[19] for Pd^{2+}–CO, Pd^+–CO, and $Pd^{\delta+}$–CO, it is suggested that the band at 2114 cm^{-1} is at the high-frequency limit of the range for Pd^0–CO, while the band at 2100 cm^{-1} is right inside this range and, therefore, is assigned to Pd^0–CO. If these assignments are correct, the bands at 2124 and 2121 cm^{-1} must be attributed to Pd^+–CO and $Pd^{\delta+}$–CO complexes, respectively, with the Pd^+ or $Pd^{\delta+}$ presumably occupying $S_{II'}$ sites and the CO ligands coordinates through the six-membered oxygen ring.[3] For samples reduced at higher temperature, the overall intensity of the terminal bands increases, as stated above, but the relative absorbance of the band at 2124 cm^{-1} decreases with respect

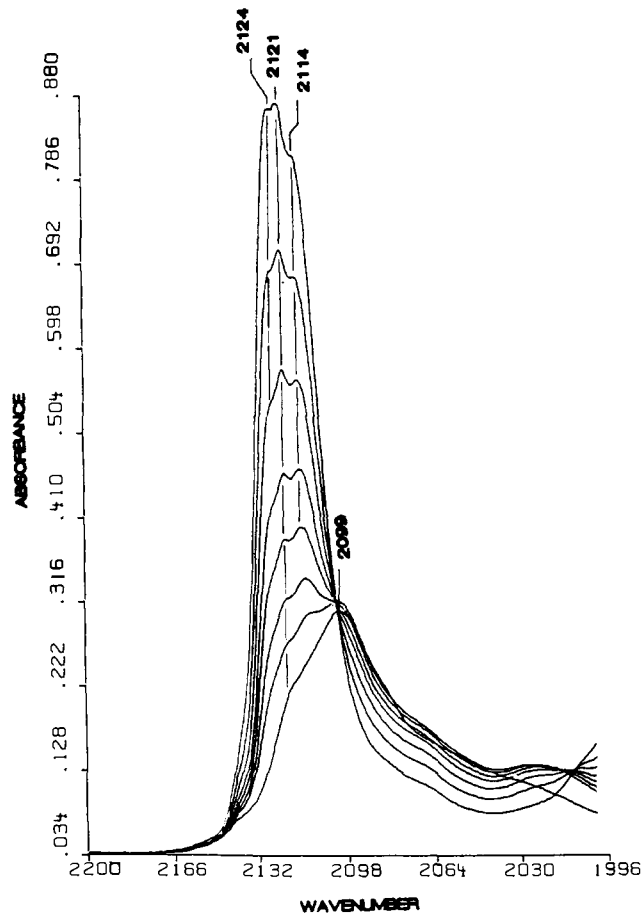

Figure 10. Detail of the terminal C–O stretching bands of Figure 1. Ar purging time (min): 20, 25, 30, 35, 40, 45, 50, 70.

to that of the 2120-cm^{-1} band. It appears only as a weak shoulder on the high-frequency side of the 2120-cm^{-1} band after reduction at 200 °C and can hardly be recognized after reduction at 350 °C. This behavior lends further credence to our assignment of the 2124-cm^{-1} band to accessible Pd^+ ions.

As mentioned, the band positions of characteristic peaks in the CO–FTIR spectra of gently reduced samples are strikingly similar to those of the corresponding peaks reported for CO on Pd single-crystal faces.[14] Our 1824-cm^{-1} band closely matches the 1823-cm^{-1} band reported for Pd(111) at low coverage; likewise, the present 1900-cm^{-1} band agrees with the 1895 cm^{-1} for CO on Pd(100), again extrapolated to low coverage[14] in order to eliminate the effect of dipole–dipole coupling at higher coverages on planar faces. This similarity of the band positions implies that the C–O bond strength and, consequently, also the chemical bonds between Pd and CO, are very similar for the present clusters and for Pd single crystals. As the heat of adsorption of CO on Pd is known to be 30 kcal/mol,[13,20] it follows that the activation energy for desorption must be equal to or larger than this, and that thermal desorption at room temperature should be very slow. This behavior is, indeed, observed for the large Pd particles (see Figure 6), but definitely not observed for the carbonyl clusters. Therefore, we conclude that the release of CO from the carbonyl clusters at room temperature cannot be a simple thermal desorption process. The changes in the spectra due to purging also cannot be attributed to a simple rehybridization, as was proposed by Yates et al.[21] for CO on Pd/SiO_2. Rehybridization would require that the high wave number band decreases while the neighboring low wave number band increases as the CO coverage decreases, which

(15) (a) Albano, V. G.; Ceriotti, A.; Chini, P.; Ciani, G.; Martinengo, S.; Anker, M. *J. Chem. Soc., Chem. Commun.* **1975**, 859. (b) Albano, V. G.; Ciani, G.; Martinengo, S.; Sironi, S. *J. Chem. Soc., Dalton Trans.* **1979**, 978.
(16) (a) Schmid, G.; Klein, N. *Angew. Chem.* **1986**, *98*, 910. (b) Schmid, G.; *Chem. Unserer Zeit* **1988**, *22*, 85.
(17) Bergeret, G.; Tri, T. M.; Gallezot, P. *J. Phys. Chem.* **1983**, *87*, 1160.
(18) Zhang, Z.; Sheu, L. L.; Sachtler, W. M. H., to be published data.
(19) (a) Palazov, A.; Chang, C. C.; Kokes, R. J. *J. Catal.* **1975**, *36*, 338. (b) Shubin, V. E.; Shvets, G. A.; Sawel'eva, G. A.; Popova, N. M.; Kazanskii, V. B.; *Kinet. Katal.* **1982**, *23*, 1153 (Engl.: *Kinet. Catal.* **1986**, *27*, 1022). (c) Juszczik, W.; Karpinski, Z.; Ratajczykowa, I.; Stanasiuk, Z.; Zielinski, J.; Sheu, L. L.; Sachtler, W. M. H., submitted for publication in *J. Catal.*

(20) Ertl, G. In *Metal Clusters in Catalysis*; Gates, D. C., Guczi, L., Knözinger, H., Eds.; Elsevier: Amsterdam, 1986; pp 507–604.
(21) (a) Gelin, P.; Siedle, A. R.; Yates, J. T., Jr. *J. Phys. Chem.* **1984**, *88*, 2978. (b) Gelin, P.; Yates, J. T., Jr. *Surf. Sci.* **1984**, *136*, L1.

is not the case for the present system. It follows that the CO release observed in the present study must be due to a chemical process of low activation energy and complete reversibility at room temperature.

These observations prompt us to propose a new model, in which Pd carbonyl clusters interact with zeolite protons. It is known that bonds between H and Pd are strong; attaching a proton to a Pd_n cluster results in the formation of a positively charged $[H-Pd_n]^+$ cluster. CO ligands are less strongly bonded to such an electron-deficient cluster; some ligands, therefore, will be released while others remain attached to the cluster, but their characteristic IR frequency will shift to higher wavenumbers. The process can be written schematically:

$$Pd_n(CO)_a + H^+ \rightarrow [H-Pd_n(CO)_x]^+ + (a-x)CO_{gas}$$

This reaction may be either thermally neutral or slightly endothermic. Entropy drives it to the right under the conditions of Ar purging, but to the left when CO is admitted. Such reactions between cluster and cage wall will be typical for small clusters inside supercages in contrast to the behavior of large Pd particles. This model is supported by the observed intensity changes of the 3647-cm^{-1} band of the zeolite O-H bond. Also this process is completely reversible: when CO is reintroduced, the proton returns to the cage wall. The stretching frequency at 1823 cm^{-1} is typical for triply bonding CO on a neutral Pd_n cluster in state I. When the cluster acquires a positive charge by reacting with a proton, back-bonding from Pd to CO is diminished; it appears, therefore, possible that in state II the new band at 1860 cm^{-1}, which is separated from the eroding bands of state I by two sharp isosbestic points, represents the stretching frequency of the triply bonded CO on the electron-deficient cluster.

Zeolite protons may also interact with the oxygen atoms of CO ligands. This would result in changes of the stretching frequencies of both the zeolite O-H and the ligand C-O bonds, both being shifted toward lower wavenumbers. Indeed, a band shift in this direction is observed for the O-H band (in addition to the previously noted lower intensity), and one might speculate that the new shoulder in state II at 2060-2100 cm^{-1} is actually a red-shifted C-O stretching frequency of the terminal CO ligand. More work, however, will be necessary to substantiate this hypothesis.

Conclusions

Pd carbonyl clusters, apparently without precedent in the literature, are formed by admitting CO at room temperature to Pd/NaY, previously reduced at low temperatures, in which the size of the Pd clusters in the supercages is limited by the width of the cage windows. The IR spectrum, showing sharp bands, of the carbonyl cluster is quite different from spectra of adsorbed CO on supported transition metals. A cluster with 13 Pd atoms in its core could be consistent with the geometric constraints in faujasite supercages. The IR spectrum changes drastically upon purging at room temperature; new bands appear, separated by isosbestic points from the waning bands. The positions of the major IR bands are very similar to those reported for CO on Pd single crystals, which implies that also the heats of adsorption should be very similar. The easy release of CO from these clusters is, therefore, incompatible with thermal desorption; it is attributed to a reaction involving zeolite protons. IR data of the zeolite O-H band support this model.

Acknowledgment. Support from the U.S. Department of Energy under Contract DE-FG02-87ERA3654 is gratefully acknowledged.

Polarized Vacuum Ultraviolet Spectra of Crystalline Urea†

Blair F. Campbell‡ and Leigh B. Clark*

Contribution from the Department of Chemistry, University of California—San Diego, La Jolla, California 92093-0342. *Received May 1, 1989*

Abstract: Polarized vacuum UV reflection spectra from single crystals of urea and a urea-hydrocarbon adduct are reported. Corresponding absorption spectra are obtained through Kramers-Kronig analysis of the reflection data. Spectra taken from the (110) face of tetragonal urea show the presence of three strong absorption bands in the 56 000- to 65 000-cm^{-1} region. The results for urea are I (56 000 cm^{-1}, $f = 0.21$, B-type molecular excited-state symmetry, II (62 000 cm^{-1}, $f = 0.23$, A_1 symmetry), and III (65 000 cm^{-1}, $f = 0.09$, B-type symmetry). Reflection data and corresponding absorption spectra taken from the hexagonal urea-hexadecane adduct exhibit the same three transitions as found in urea, and in addition can be used to distinguish between $A_1 \rightarrow B_1$ and $A_1 \rightarrow B_2$ molecular transitions. The result is that both B-type excited states are of B_2 symmetry species. The effects of exciton mixing on the urea spectra are considered and found to be of minor importance. The experimental assignments differ significantly with the results from either of the two published theoretical calculations of the electronic spectrum of urea.

In spite of the historical fact that urea was the first laboratory synthesized organic molecule,[1] very little is known about its electronic spectrum. This lack is so despite its small-molecule nature (Figure 1), its relatively high symmetry (C_{2v}), and its candidacy as a fertile testing ground of theories aimed at understanding the electronic structure of the many important molecules made up of C, N, and O atoms. As far as we know, there have been published but two attempts at calculating the electronic spectrum of urea. The first calculation using a valence bond approach involving "interlocking amide resonance" was published by Rosa and Simpson[2] in 1964 and was followed by an ab initio calculation by Elbert and Davidson[3] in 1974. Experimental information is scant. Ley and Arends[4] reported a featureless onset of absorption in aqueous solution in the 180-185-nm range. An absorption spectrum of urea dissolved in trimethyl phosphate showing a single structureless absorption band centered at 58 800 cm^{-1} can be found in the doctoral dissertation of Rosa.[5] In addition, a spectrum of urea obtained by the SF_6 scavenger technique has been reported.[6]

†This work was supported by a National Institutes of Health grant (GM38575).

‡Present address: Rocketdyne Division, Rockwell International Corp., 6633 Canoga Ave., Canoga Park, CA 91303.

(1) Lipman, T. O. *J. Chem. Educ.* **1964**, *41*, 452.
(2) Rosa, E. J.; Simpson, W. T. In *Physical Processes in Radiation Biology*; Augenstein, L., Mason, R., Rosenberg, B., Eds.; Academic Press: New York, 1964; p 43.
(3) Elbert, S. T.; Davidson, E. R. *Int. J. Quantum. Chem.* **1974**, VIII, 857.
(4) Ley, H.; Arends, B. *Z. Phys. Chem.* **1932**, *B17*, 177.
(5) Rosa, E. J. Doctoral Dissertation, University of Washington, 1964.

0002-7863/89/1511-8131$01.50/0